Path Following of a Quadrotor with a Cable-Suspended Payload

Adeel Akhtar, *Member IEEE*, Sajid Saleem, *Senior Member IEEE*,
and Jinjun Shan, *Senior Member IEEE*

***Abstract*—This paper addresses the design of a path following controller for a payload tethered to a quadrotor. Specifically, the goal is to design a smooth dynamic feedback controller that forces the suspended payload to converge and follow a large class of embedded curves. The given curve is treated as a smooth manifold, and set stabilization is used to find the maximal control invariant manifold. The controller design guarantees that once the aerial robot approaches the path, the payload never leaves the path. The performance of the proposed controller is verified through simulations with practical sensor noise and parametric uncertainties. Moreover, experimental implementation and verification of the proposed control scheme are performed on a Quanser UAV platform in an indoor flying arena.**

***Index Terms*—Nonlinear controls, path following, mobile robotics, set stabilization, underactuated system, UAV**

I. Introduction

MOBILE robots, in particular unmanned aerial vehicles (UAVs), are in the spotlight because of their vast range of applications, simple mechanical design, low-cost structure, vertical take-off and landing (VTOL) ability, and agile dynamics [1]. In recent years, there has been an increased demand for efficient aerial transportation of light to the medium payload (up to a few kilograms), and a quadrotor can be an excellent choice for such a mission due to its compact size and relatively higher thrust generation capability [2].

Broadly speaking, there are two approaches to attaching a payload with a quadrotor, i.e., active and passive attachment [3]. The former approach requires a gripper attached to the body of the quadrotor that provides an additional degree of freedom. However, it comes at the cost of loss of agility due to an increase in inertia. The passive attachment uses a cable attached to the quadrotor at one end and the load to the other end. The cable suspension approach provides an agile platform and better manoeuvrability [4], [5]; however, it brings its challenges to the controller design because of an additional degree of under-actuation [6].

A. Akhtar and J. Shan are with with the Department of Earth and Space Science and Engineering, York University, 4700 Keele Street, Toronto, ON, Canada M3J 1P3. {a5akhtar;jjshan}@yorku.ca

S. Saleem is with the Department of Computer and Network Engineering, College of Computer Science and Engineering, University of Jeddah, Jeddah 23890, Saudi Arabia. sssaleem@uj.edu.sa

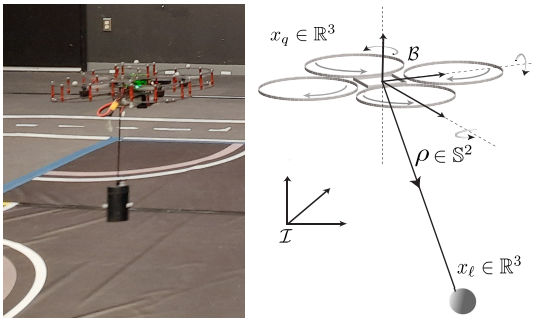

Fig. 1. Experimental setup and a schematic of a quadrotor with a cable-suspended payload.

In this paper, we consider a path following problem for the system consisting of a quadrotor attached with a cable-suspended load, as shown in Figure 1. Given a differentiable curve, satisfying certain assumptions, in three-dimensional space and a quadrotor system attached with a cable-suspended load, the goal is to design a smooth controller that forces the payload to converge to the desired path and follow it. Unlike a trajectory, a path is a set of points without a timing law associated with it. In literature, a path and a trajectory are used interchangeably. However, we underscore that a path could be viewed as a collection of trajectories [7]. Thus, a path following problem is more general than a trajectory tracking problem in this sense. As observed in [8]–[11], there exist scenarios where the trajectory tracking approach leads to certain performance limitations, while a satisfactory solution can be achieved through the path following approach. A primary feature of the path following scheme is that the closed-loop system can attain path invariance. In other words, once the system approaches the assigned path, it never leaves the path [7].

It is well known that the configuration space of a quadrotor or a quadrotor attached with a cable-suspended load is a smooth manifold [12]. In literature, approaches to the design of a controller for non-linear systems evolving on a manifold can be classified into coordinate free (or geometric) and local coordinate-based methods [13]. The geometric methods employ a hierarchical controller design framework based upon an inner-outer loop approach, which provides singularity-free control laws [14]–[17]. The inner loop stabilizes the system's attitude, whose convergence is followed by the convergence of the outer loop, which stabilizes the position of the load.

Although this cascade control design method leads to a simpler design approach, the stability of the individual loops does not automatically guarantee the convergence of the overall system, for which the stability must be justified independently. One of the shortcomings of most prior geometric controllers applied to the system under consideration is that these methods are designed to track a curve, which is parameterized by time, i.e., a trajectory [3], [15], [17]–[19]. As demonstrated in [8], the trajectory tracking approach has performance limitations and fails to guarantee path invariance [5], [8]. The second approach, i.e., the coordinate-based method using local charts, leads to local controllers that suffer singularities, such as gimbal lock [4], [20]. Despite this constraint, a large class of both closed and non-closed curves can be followed without approaching singularity [21].

In this paper, we consider a local coordinate-based approach, i.e., Euler angle representation; therefore, to no surprise, our results are local [21]. However, unlike existing approaches applied to the design of controllers for the system with a quadrotor and a suspended load, we do not follow a cascade (inner-outer loop) structure and instead propose a monolithic approach. Unlike most existing work, we adopt a monolithic design approach for the UAV system with cable-suspended load, which guarantees path invariance for a class of functions in the output space. This monolithic scheme does not demand time separation between UAV rotational and translational dynamics. Furthermore, any time-scale separation between the payload and the UAV is not required [10]. Another advantage of our proposed controller is the guarantee it provides about path invariance while the payload attains some auxiliary user-defined constraints about position, velocity or acceleration.

It must be emphasized that, unlike "standard" feedback linearization approaches that linearize the system with respect to the output variables only, our approach provides a general linearizing transformation for a set of smooth functions in the output space that satisfy conditions specified in (14). As an instance, the output variables used for feedback linearization in [3] are a special case of our proposed class of linearizing functions.

We have made the following contributions.

1) We have designed a dynamic transverse feedback linearizing controller that allows the cable-suspended load attached to the quadrotor to follow a large class that consists of closed and non-closed paths.
2) Unlike standard feedback linearization methods, we demonstrate for a large class of curves that the closed loop system exhibits a well-defined vector relative degree (Theorem IV.5), and have proved that after dynamic extension, the system is diffeomorphic to a chain of integrators (Corollary IV.6).
3) Experimental verification of our feedback controller is performed by implementing it on a UAV, i.e., Quanser Qdrone (Section VI).

In [22], the authors consider a path following problem and propose an inner-outer loop control approach. The key limitation of their work is that the system can only follow straight lines. For non-straight paths, a piece-wise approximation is computed, and hence the controller requires switching.

A. Notation and math preliminaries

The n-dimensional Euclidean space is represented by $\mathbb{R}^n$ and each of its elements is an ordered n-tuple $(x_1, \ldots, x_n)$. Column vectors are denoted by $x = \mathrm{col}(x_1, \ldots, x_n)$, for $x \in \mathbb{R}^n$. An i-dimensional column vector consisting of all zeros is denoted by 0_i. For a linear transformation $A \in \mathbb{R}^{m\times n}$, $A^\top \in \mathbb{R}^{n\times m}$ represents its transpose. For Euclidean space, the inner product and norm are represented by $\langle\cdot,\cdot\rangle$ and $\|\cdot\|$, respectively. For a set $A \subset \mathbb{R}^n$ and point $p \in \mathbb{R}^n$, the point-to-set distance is given by $\|x\|_A := \inf_{q\in A} \|p-q\|$. The cross product between two vectors in $\mathbb{R}^3$ is represented by $\times$. The composition of two maps, $h : A \to B$ and $s : B \to C$, is represented by $s \circ h : A \to C$. A curve $\sigma : \mathbb{D} \to \mathbb{R}^n$ is a parameterized curve such that its domain is $\mathbb{D} = \mathbb{R}$ if it is non-closed. However, for a parameterized curve σ that is closed with period T, $\sigma(\lambda+T) = \sigma(\lambda)$ and its domain is $\mathbb{D} = \mathbb{R} \bmod T$. The derivative of the curve σ with respect to the path parameter λ is denoted by σ'. For a continuously differentiable function $f : \mathbb{R}^n \to \mathbb{R}^m$ and $p \in \mathbb{R}^n$, its derivative f at p is expressed by $df_p := \frac{\partial f}{\partial x}\Big|_{x=p}$. For smooth maps $f, g : \mathbb{R}^n \to \mathbb{R}^n$ and a smooth map $\lambda : \mathbb{R}^n \to \mathbb{R}$, the iterative Lie derivatives are defined as $L_g^0\lambda := \lambda$, $L_g^k\lambda := L_g(L_g^{k-1}\lambda)$, $L_gL_f\lambda := L_g(L_f\lambda)$. Consider a smooth vector field $f : \mathbb{R}^n \to \mathbb{R}^n$ and the solution curve $x : \mathbb{R} \to \mathbb{R}^n$ to the initial value problem $\dot{x}(t) = f(x(t))$, $x(0) = x_0$. Then the flow of the smooth vector field f is given by $\phi(x_0, t) = x(t)$.

II. Dynamic Model

In this article, we consider a quadrotor and a payload, which is attached to the center of gravity of the quadrotor by a cable. We made the following assumption.

Assumption 1. *The cable has zero mass and is non-stretchable. The mass of the payload, which is assumed to be a point-mass, is less than the payload capacity of the quadrotor. Furthermore, the tension in the cable is assumed to be positive for all time* [1].

Let $\mathcal{I} := \{e_1, e_2, e_3\}$ be the fixed inertial frame and $\mathcal{B} := \{b_1, b_2, b_3\}$ be the body frame attached to the center of mass of the quadrotor. Let $x_q(t) \in \mathbb{R}^3$ and $x_\ell(t) \in \mathbb{R}^3$ represent the position of the quadrotor and payload, respectively. Similarly, $v_q(t) \in \mathbb{R}^3$ and $v_\ell(t) \in \mathbb{R}^3$ be the velocity of the quadrotor and the payload, respectively. Let $m_q \in \mathbb{R}$ and $m_\ell \in \mathbb{R}$ and be the mass of the quadrotor and payload, respectively, and $g \in \mathbb{R}$ be the acceleration due to gravity. Let $b_3 = \mathrm{col}(0, 0, 1)$ be the unit vector in z direction. The non-zero total thrust of the quadrotor is represented by the scalar $u_t(t)$. Let $\rho(t) \in \mathbb{S}^2$ be the unit vector from the quadrotor to the load. Let $L \in \mathbb{R}$ and $T > 0 \in \mathbb{R}$ be the length of the cable and its tension, respectively. The position of the quadrotor and the position of the load are related by

$$x_q(t) = x_\ell(t) - L\rho(t). \tag{1}$$

[1] For a model that allows non-negative tension in the cable, hybrid control techniques can be used to design a controller, for details see [23].

Let $\Omega(t) := \text{col}(\Omega_1(t), \Omega_2(t), \Omega_3(t)) \in \mathbb{R}^3$ be the body rates of the quadrotor, $J := \text{diag}(J_x, J_y, J_z) \in \mathbb{R}^{3\times3}$ be the inertia of the quadrotor with respect to the three axes of $\mathcal{B}$. Similarly, we define the total input torque by $\tau(t) := \text{col}(\tau_1(t), \tau_2(t), \tau_3(t)) \in \mathbb{R}^3$, which along with the thrust $u_t(t)$ constitute the four inputs of the system under consideration. We assume that the orientation $R(t) \in \mathsf{SO}(3)$ of the quadrotor is represented locally by three Euler angles, i.e., roll-pitch-yaw $\Phi(t) := \text{col}(\phi(t), \theta(t), \psi(t)) \in \mathbb{R}^3$. The dynamics of the quadrotor with a cable-suspended load [12], [23], can be locally represented[2] as

$$\begin{aligned}
\dot{x}_\ell &= v_\ell \\
\dot{v}_\ell &= -\frac{T}{m_\ell L}(x_\ell - x_q) - g b_3 \\
\dot{x}_q &= v_q \\
\dot{v}_q &= \frac{u_t}{m_q} R b_3 - g b_3 + \frac{T}{m_q L}(x_\ell - x_q) \\
\dot{\Phi} &= M\Omega \\
\dot{\Omega} &= J^{-1}\left(\tau - (\Omega \times J\Omega)\right),
\end{aligned} \tag{2}$$

where M and R matrices are defined in terms of Euler angles (for details, see [24]). Note that the state vector for the above-mentioned system is $\text{col}(x_\ell, v_\ell, x_q, v_q, \Phi, \Omega) := x := \text{col}(x_1, \cdots, x_{18}) \in \mathbb{R}^{18}$, and the input vector is $\text{col}(\tau_1, \tau_2, \tau_3, u_t) \in \mathbb{R}^4$. The output of system (2) is the position of the point-mass and is given by

$$y = h(x) = x_\ell, \tag{3}$$

where $h : \mathbb{R}^{18} \to \mathbb{R}^3$ is a smooth map.

III. Problem Statement

As mentioned previously, the path following and trajectory following problems are not identical. Specifically, a trajectory is a time-parameterized curve, while a path consists of a set of points in the output space without any time specification. In this section, we formally define the path following problem for a payload suspended to a quadrotor. The objective is to force the payload to approach an assigned path and then maintain its position on this path subsequently.

Let us consider a curve γ parameterized by λ

$$\begin{aligned}
\sigma : \mathbb{D} &\to \mathbb{R}^3 \\
\lambda &\mapsto \text{col}\left(\sigma_1(\lambda), \sigma_2(\lambda), \sigma_3(\lambda)\right).
\end{aligned}$$

Moreover, the given curve is assumed to be a regular curve, i.e., a smooth non-intersecting curve. Mathematically, a regular curve satisfies $\|\sigma'(\lambda)\| \neq 0$ for all $\lambda \in \mathbb{D}$. For all regular curves, its possible to find a unit-speed parameterization [7]. We assume that the parameterization σ of the curve is a unit speed parameterization, i.e., $\|\sigma'(\lambda)\| = 1$. Next, we consider the following technical assumption [21].

Assumption 2. *The curve $\gamma \subset \mathbb{R}^3$ is one-dimensional embedded submanifold[3]. For an open set V, a smooth function $s : V \subset \mathbb{R}^3 \to \mathbb{R}^2$ exists such that $\gamma = s^{-1}(0)$ with $\text{rank}\,(ds_y) = 2$, for all $y \in \gamma$.*

Since $\gamma = s^{-1}(0)$, for the cable-suspended UAV system (2), the zero-level representation of the path is given as

$$\gamma := s^{-1}(0) = \left\{y \in \mathbb{R}^3 : s_1(y) = s_2(y) = 0\right\}.$$

Informally, the above assumption restricts the choice of paths to non-self intersecting smooth curves.

Problem 1. *Consider the system (2) and a given curve γ satisfying Assumption 1 and Assumption 2, respectively, design a dynamic smooth feedback-control law*

$$\begin{aligned}
\dot{z} &= \mathcal{A}(x,z) + \mathcal{B}(x,z)u \\
\begin{bmatrix}\tau \\ u_t\end{bmatrix} &= \mathcal{C}(x,z) + \mathcal{D}(x,z)u,
\end{aligned} \tag{4}$$

where $u \in \mathbb{R}^4$ and $z \in \mathbb{R}^k$, such that if the UAV system with the point-mass load initializes in the neighbourhood $\mathcal{U} \times \mathcal{V} \subset \mathbb{R}^{18} \times \mathbb{R}^k$ and $\gamma \subset h(\mathcal{U})$, the system meets the below-mentioned goals:

- **G1** *for any initial condition $(x(0), z(0)) \in \mathcal{U} \times \mathcal{V}$, the output of the system asymptotically approaches the path, i.e., $\|h(x(t))\|_\gamma \to 0$, as $t \to \infty$;*
- **G2** *the curve $\gamma := s^{-1}(0)$ achieves path invariance, for all $t \geq 0$;*
- **G3** *on the curve γ, the point-mass and the UAV meet auxiliary application-specific requirements such as point stabilization of the payload or the speed along the curve.*

IV. Dynamic control design

For a UAV system with a cable-suspended payload, our goal is to control the payload position x_ℓ and UAV heading ψ. Therefore, we define the augmented-output of (2) as

$$\bar{y} := \bar{h}(x_\ell, \psi) = \bar{h}(x_1, x_2, x_3, x_{15}) \in \mathbb{R}^4. \tag{5}$$

Next, we demonstrate that, for any smooth function of the augmented output space (5), the system (2) does not possess a well-defined vector relative degree, see Definition VIII.1. To be precise, let $\alpha_i : \mathbb{R}^3 \to \mathbb{R}$, $x_\ell \mapsto \alpha_i(x_\ell)$ for $i \in \{1,2,3\}$ be smooth real-valued functions and $\alpha_4 : \mathbb{R}^4 \to \mathbb{R}$, $(x_\ell, \psi) \mapsto \alpha_4(x_\ell, \psi)$ be another smooth real-valued function. To this end, we construct a virtual output function as

$$\bar{y} = \text{col}\left(\ \alpha_1(x_\ell), \alpha_2(x_\ell), \alpha_3(x_\ell), \alpha_4(x_\ell, \psi)\ \right). \tag{6}$$

The following result shows that there does not exist any smooth function of the form $\bar{y}$ in $\mathbb{R}^4$ that would guarantee a well-defined relative degree of the system.

Lemma IV.1. *System (2) with the output function (6) does not achieve a well-defined vector relative degree for any $x \in \mathbb{R}^{18}$.*

Intuitively, the singular decoupling matrix in Lemma IV.1 corresponds to the vanishing flow of the output vector $\bar{y}$ in the direction of the vector field $\bar{g}_1$. The invertibility of the decoupling matrix can be achieved by dynamic extension [10].

[2] note that the argument t is dropped for notational simplicity

[3] Informally, a non-self-intersecting curve is an embedded submanifold.

Let $u_t = z_1$, $\dot{z}_1 = z_2$, and $\dot{z}_2 = u_d$, where u_d is our new control input obtained with the help of two integrators, i.e.,

$$\begin{aligned} \dot{z}_1 &= z_2 \\ \dot{z}_2 &= u_d. \end{aligned} \tag{7}$$

Let $u = \text{col}(u_1, u_2, u_3, u_4) := \text{col}(\tau_1, \tau_2, \tau_3, u_t)$. The dynamic extension leads to the following extended system:

$$\begin{aligned} \dot{x}_\ell &= v_\ell \\ \dot{v}_\ell &= -\frac{T}{m_\ell L}(x_\ell - x_q) - g b_3 \\ \dot{x}_q &= v_q \\ \dot{v}_q &= \frac{z_1}{m_q} R b_3 - g b_3 + \frac{T}{m_q L}(x_\ell - x_q) \\ \dot{\Phi} &= M\Omega \\ \dot{\Omega} &= J^{-1}(\tau - (\Omega \times J\Omega)) \\ \dot{z}_1 &= z_2 \\ \dot{z}_2 &= u_d. \end{aligned} \tag{8}$$

To simplify notation, we do not distinguish among the states of system (2) and the states of the controller (7), i.e., $(x_1, \ldots, x_{18})$ and (z_1, z_2). Let $x_{19} := z_1$ and $x_{20} := z_2$. Thus, for the extended system (8), the state vector is defined as $\mathbf{x} := \text{col}(x_\ell, v_\ell, x_q, v_q, \Phi, \Omega, z_1, z_2) = \text{col}(x_1, \ldots, x_{20}) \in \mathbb{R}^{20}$. Let

$$f(\mathbf{x}) := \text{col}\left(v_\ell, -\frac{T}{m_\ell L}(x_\ell - x_q) - g b_3, v_q, \frac{z_1}{m_q} R b_3 - g b_3 + \frac{T}{m_q L}(x_\ell - x_q), M\Omega, J^{-1} - (\Omega \times J\Omega), 0, 0\right),$$

$g_1(\mathbf{x}) := \text{col}\left(0_{15}, \frac{1}{J_x}, 0_4\right)$, $g_2(\mathbf{x}) := \text{col}\left(0_{16}, \frac{1}{J_y}, 0_3\right)$, $g_3(\mathbf{x}) := \text{col}\left(0_{17}, \frac{1}{J_z}, 0_2\right)$, and $g_4(\mathbf{x}) := \text{col}\,(0_{19}, 1)$ in $\mathbb{R}^{20}$, be smooth vector fields, then the extended system (8) can be expressed compactly in the control-affine form

$$\dot{\mathbf{x}} = f(\mathbf{x}) + \sum_{i=1}^{4} g_i(\mathbf{x}) u_i. \tag{9}$$

To achieve the first two objectives of the path following problem, i.e., **G1** and **G2**, we employ the zero-level set form of the desired path γ and write

$$\begin{bmatrix} \alpha_1(x) \\ \alpha_2(x) \end{bmatrix} := s \circ h(x) = \begin{bmatrix} s_1 \circ h(x) \\ s_2 \circ h(x) \end{bmatrix}, \tag{10}$$

so that $\frac{\partial \alpha_i}{\partial x_j} = 0$, for $i \in \{1, 2\}$, and $j \in \{4, 5, \ldots, 18\}$. Informally, the smooth functions α_1 and α_2 depend only on x_ℓ. Next, we lift the desired path γ to the UAV with payload system's state space. As a consequence, we obtain a submanifold of $\mathbb{R}^{20}$, i.e.,

$$\Gamma := \left\{\mathbf{x} \in \mathbb{R}^{20} : s_1(h(x)) = s_2(h(x)) = 0\right\}.$$

As the system states $\mathbf{x} \in \mathbb{R}^{20}$ converge to the lifted set Γ, the point-mass position x_ℓ asymptotically reaches the given path γ. It must be noted that the set Γ is not an invariant set for the system (8), therefore, even if the states converge to this set, they may leave afterwards. Now, we seek the largest invariant set contained inside Γ and name it as the path following manifold [9].

Definition IV.2. *For a desired path γ, the path-following manifold $\Gamma^\star$ of (8) is the maximal controlled invariant submanifold contained in the lift of γ. Furthermore, $\Gamma^\star \subset \Gamma$ and $\Gamma^\star \neq \emptyset$.*

We can apply the zero dynamics algorithm to determine the path following manifold, which is given by

$$\Gamma^\star = \left\{\mathbf{x} \in \mathbb{R}^{20} : \alpha_i(x) = \ldots = \alpha_i^{(6)}(x) = 0, \forall i \in \{1, 2\}\right\}.$$

Intuitively, the path following manifold $\Gamma^\star$ consists of all maneuvers of the system under consideration such that there exists an input signal that makes the set $\Gamma^\star$ invariant. Next, we present two results to establish the stability of the path following manifold $\Gamma^\star$.

Lemma IV.3 ([21]). *For three linearly independent vectors v_1,v_2, and v_3 all in $\mathbb{R}^3$, $\langle v_1, (v_2 \times v_3)\rangle \neq 0$.*

Given σ and α_i defined in Section III and Section IV, respectively, let $d_{x_\ell}\alpha_i := \text{col}(\frac{\partial \alpha_i}{\partial x_1}, \frac{\partial \alpha_i}{\partial x_2}, \frac{\partial \alpha_i}{\partial x_3})$, for $i \in \{1, 2\}$, and let $\sigma' := \text{col}(\frac{\partial \sigma_1}{\partial \lambda}, \frac{\partial \sigma_2}{\partial \lambda}, \frac{\partial \sigma_3}{\partial \lambda})$.

Lemma IV.4 ([25]). *Given two smooth maps α_1 and α_2, as defined in (10), $\text{span}\{d_{x_\ell}\alpha_1, d_{x_\ell}\alpha_2, \sigma'\} = \mathbb{R}^3$ for all $x_\ell \in \gamma$.*

Proof. For proof, see Appendix VIII-A. □

To solve the path following problem, we need to select four functions in the output space. Two of these functions, i.e., α_1 and α_2 have already been defined in (10) and will help us achieve the goals **G1** and **G2** of the path following problem. To meet **G3**, we define another function α_3 in the output space by exploiting the parametric representation of the given curve γ. Let $\mathcal{N}(\gamma) \subset \mathbb{R}^3$ be an open set containing the path γ such that given an element $y \in \mathcal{N}(\gamma)$, a unique $y^\star \in \gamma$ exists that it satisfies $\|y\|_\gamma = \|y - y^\star\|$. Next, we define a smooth map:

$$\begin{aligned} \varpi : \mathcal{N}(\gamma) &\to \mathbb{D} \\ y &\mapsto \arg\inf_{\lambda \in \mathbb{D}} \|y - \sigma(\lambda)\|. \end{aligned} \tag{11}$$

This definition leads to the map α_3, which is given as

$$\alpha_3 := \varpi \circ h : \mathbb{R}^{18} \to \mathbb{R}. \tag{12}$$

Finally, we select the fourth function to control the UAV's heading, i.e.,

$$\begin{aligned} \alpha_4 : \mathbb{R}^4 &\to \mathbb{R} \\ (x_\ell, \psi) &\mapsto \alpha_4(x_\ell, \psi), \end{aligned} \tag{13}$$

such that α_4 is smooth and $\partial_\psi(\alpha_4) \neq 0$, for all $\mathbf{x} \in \mathbb{R}^{20}$. In summary, given α_1 and α_2 satisfying Lemma IV.4, α_3 defined in (12), and α_4 defined in (13), we construct a refined virtual output function

$$\overline{y} = \begin{bmatrix} \alpha_1(x) \\ \alpha_2(x) \\ \alpha_3(x) \\ \alpha_4(x_\ell, \psi) \end{bmatrix} = \begin{bmatrix} s_1 \circ h(x) \\ s_2 \circ h(x) \\ \varpi \circ h(x) \\ \alpha_4(x_\ell, \psi) \end{bmatrix}. \tag{14}$$

Next, we determine the vector relative degree [26, Def. 9.15] of the UAV system and the cable-suspended payload.

Theorem IV.5. *Given the system model in* (9) *and a path satisfying* Assumption 1 *and* Assumption 2*, respectively, and a virtual output function given in* (14)*, the system has a well-defined vector relative degree* $\{6,6,6,2\}$ *everywhere on the set* $\Gamma^\star \cap \{\mathbf{x} \in \mathbb{R}^{20} : x_{19} \neq 0, \cos(x_{13}) \neq 0, \cos(x_{14}) \neq 0\}$.

Proof. Let us consider an $x^\star \in \Gamma^\star$ and determine the path parameter $\lambda^\star \in \mathbb{D}$ such that it satisfies $h(x^\star) = \sigma(\lambda^\star)$. It follows from Definition IV.2 that $\Gamma^\star \subseteq \Gamma$ and the output $h(x^\star)$ is on the assigned curve γ. To determine the vector relative degree, we need to show that for each x in a neighbourhood of $x^\star$

$$L_{g_i} L_f^j \alpha_k(x) \equiv 0, L_{g_i}\alpha_4(x) \equiv 0,$$

for $i \in \{1,2,\ldots,4\}$, $j \in \{0,1,\ldots,4\}$, $k \in \{1,2,3\}$ and the 4×4 decoupling matrix

$$D(x) = \begin{bmatrix} L_{g_1}L_f^5\alpha_1(x) & \ldots & L_{g_4}L_f^5\alpha_1(x) \\ L_{g_1}L_f^5\alpha_2(x) & \ldots & L_{g_4}L_f^5\alpha_2(x) \\ L_{g_1}L_f^5\alpha_3(x) & \ldots & L_{g_4}L_f^5\alpha_3(x) \\ L_{g_1}L_f\alpha_4(x) & \ldots & L_{g_4}L_f\alpha_4(x) \end{bmatrix}, \tag{15}$$

is full rank. Direct calculation of Lie derivatives yield

$$L_{g_i} L_f^j \alpha_k(x) = 0, L_{g_i}\alpha_4(x) = 0.$$

To demonstrate the invertibility of the decoupling matrix, we derive its determinant, which can be simplified as

$$\det(D(x)) = \left(\frac{T^3 x_{19}^2 \cos(x_{13})}{\det(J) L^3 m_\ell^3 m_q^3 \cos(x_{14})}\right)(\partial_\psi \alpha_4) \langle d_{x_\ell}\alpha_1, (d_{x_\ell}\alpha_2 \times \sigma')\rangle. \tag{16}$$

The matrix $D(x)$ is singular when either the numerator of (16) is zero or the denominator is unbounded. Note that the determinant of the diagonal inertia matrix J is finite since all the parameters on its diagonal are finite. Moreover, m_q and m_ℓ are the mass of UAV and payload, respectively, which are finite positive constants. By Assumption 1, cable tension $T \neq 0$. The term $\cos(x_{14})$ is bounded and is therefore finite; the physical parameter L, which is the length of cable, is non-zero. By Lemma IV.4, the $\text{span}\{d_{x_\ell}\alpha_1, d_{x_\ell}\alpha_2, \sigma'\} = \mathbb{R}^3$. By Lemma IV.3, $\langle d_{x_\ell}\alpha_1, (d_{x_\ell}\alpha_2 \times \sigma')\rangle \neq 0$. Furthermore, by definition, $\partial_\psi \alpha_4 \neq 0$. As a result, we have shown that $\det(D(x)) \neq 0$, for all $x^\star \in \Gamma^\star \cap \{\mathbf{x} \in \mathbb{R}^{20} : x_{19} \neq 0, \cos(x_{13}) \neq 0, \cos(x_{14}) \neq 0\}$, and the given system (9) exhibits a well-defined vector relative degree equal to $\{6,6,6,2\}$. □

The above result leads to a coordinate transformation that converts the given system to an exact linear form.

Corollary IV.6. *Let* $x^\star \in \Gamma^\star \backslash \{\mathbf{x} \in \mathbb{R}^{20} : x_{13} = x_{14} = \pm\pi/2, x_{19} = 0\}$*. There exists a neighbourhood* $U \subset \mathbb{R}^{20}$ *containing* $x^\star$ *such that the coordinate transformation* $\mathscr{T} : U \subset \mathbb{R}^{20} \to \mathscr{T}(U) \subset \mathbb{R}^{20}$*, defined by*

$$\begin{bmatrix} \xi_i \\ \zeta_i \\ \eta_i \\ \mu_j \end{bmatrix} = \mathscr{T}(x) = \begin{bmatrix} L_f^{i-1}\alpha_1(x) \\ L_f^{i-1}\alpha_2(x) \\ L_f^{i-1}\alpha_3(x) \\ L_f^{j-1}\alpha_4(x) \end{bmatrix}, \tag{17}$$

for $i \in \{1,2,\ldots,6\}$ *and* $j \in \{1,2\}$ *is a diffeomorphism.*

Proof. Proof omitted due to space limitations. For details, see [24]. □

The diffeomorphism $\mathscr{T}$ from Corollary IV.6 allows us to express the system in term of transformed states $(\xi, \zeta, \eta, \mu) \in \mathbb{R}^{20}$ using the feedback transformation

$$\begin{bmatrix} u_1 \\ u_2 \\ u_3 \\ u_4 \end{bmatrix} := D^{-1}(x) \left(\begin{bmatrix} -L_f^6\alpha_1 \\ -L_f^6\alpha_2 \\ -L_f^6\alpha_3 \\ -L_f^2\alpha_4 \end{bmatrix} + \begin{bmatrix} v^\xi \\ v^\zeta \\ v^\eta \\ v^\mu \end{bmatrix} \right), \tag{18}$$

where $(v^\xi, v^\zeta, v^\eta, v^\mu)$ are auxiliary control inputs. By Theorem IV.5, this controller (18) is well-defined in a neighbourhood of every $x^\star \in \Gamma \backslash \{\mathbf{x} \in \mathbb{R}^{20} : x_{13} = x_{14} = \pm 90^\circ\}$. This means that in a neighbourhood of the path γ, the quadrotor system with the cable-suspended payload (8) is reduced to four decoupled chain of integrators.

$$\begin{array}{cccc} \dot{\xi}_1 = \xi_2 & \dot{\zeta}_1 = \zeta_2 & \dot{\eta}_1 = \eta_2 & \dot{\mu}_1 = \mu_2 \\ \dot{\xi}_2 = \xi_3 & \dot{\zeta}_2 = \zeta_3 & \dot{\eta}_2 = \eta_3 & \dot{\mu}_2 = v^\mu. \\ \vdots & \vdots & \vdots & \\ \dot{\xi}_6 = v^\xi & \dot{\zeta}_6 = v^\zeta & \dot{\eta}_6 = v^\eta & \end{array} \tag{19}$$

The above system consists of four decoupled linear time invariant (LTI) systems and any linear control technique can be used to stabilize (19). We call the first chain of integrators ξ-subsystem, the second chain of integrators ζ-subsystem, the third chain of integrators η-subsystem and fourth chain of integrators μ-subsystem. The output (14) is a flat output [21] for the quadrotor system with a load (8) because these outputs transform the system to a fully linear system. The linear form of the system in the transformed coordinates simplifies the design of path following controllers. It is intuitive to see that, in order to bring the system on the set Γ, we exponentially stabilize ξ- and ζ-subsystem by the following controllers:

$$v^\xi = \sum_{i=1}^{6} k_i^\xi \xi_i, \quad \text{and} \quad v^\zeta = \sum_{i=1}^{6} k_i^\zeta \zeta_i, \tag{20}$$

with appropriate values of gains k_i^ξ, and k_i^ζ, which can be determined by pole placement or similar other LTI system techniques. When all the ξ and ζ states are zero, the system converges to the path, i.e., **G1** and **G2** are satisfied and path invariance is achieved.

To fulfill the objective of making the cable-suspended load stop along the path, controlling the speed of the suspended load along the curve, or forcing the cable-suspended load to follow a given acceleration profile, jerk and high derivatives along the curve, we design the linear controller of the form

$$v^\eta = \sum_{i=1}^{6} k_i^\eta (\eta_i - \eta_i^{ref}), \tag{21}$$

where the gain k_i^η can be determined using pole placement or similar linear control techniques.

It should be noted that η_1 specifies the position of the payload along the path. By selecting η_1^{ref} as the target value, point stabilization of the suspended load along the path is achieved. By setting $k_1^\eta = 0$, and selecting η_2^{ref} as the target

TABLE I
SYSTEM PARAMETERS

Description	Physical value
mass of the quadrotor m_q	0.85 kg
mass of the payload m_ℓ	0.13 kg
inertia of the quadrotor $J = \text{diag}(J_x, J_y, J_z)$	(0.01,0.0082,0.0148) kg.m^2
maximum payload capacity	0.3 kg

velocity profile, the suspended load follows the desired profile along the curve. Similarly, by selecting $k_1^\eta = k_2^\eta = 0$, and setting η_3^{ref} to the reference acceleration profile, the suspended payload follows the desired profile. In other words, the linear controller given by (21) satisfies **G3**.

The heading angle of the quadrotor ψ can be controlled by designing a similar linear controller for the μ-subsystem

$$v^\mu = k_1^\mu(\mu_1 - \mu_1^{ref}) + k_2^\mu \mu_2, \tag{22}$$

where the gains can be selected using linear control techniques. This controller allows to achieve a given reference profile for the yaw angle, and as a consequence, the closed-loop system achieves objective **G3**. In summary, the coordinate and feedback transformations (17), (18) convert the system (8) into an exact linear form, and the auxiliary linear controllers (20), (21), and (22) satisfy **G1-G3**, and hence, path following problem is solved. The overall control scheme is shown in Figure 2.

V. SIMULATION RESULTS

This section discusses the path following simulation results for non-closed curves in the presence of additive white Gaussian noise and parametric uncertainty. To make the simulation realistic, we selected system parameters to match an actual drone, as shown in Table I. A cable length of 1m is used in the simulation scenario. Parametric uncertainties are assumed to be 10% in the measurement of the quadrotor's inertia matrix [10]. On the other hand, we assume that the uncertainty in the measurement of the two masses, i.e., m_q, m_ℓ and the cable length L is only 1% since these values can be measured precisely.

Given a non-closed regular curve $\lambda \mapsto \text{col}(\lambda, \sin(\lambda), 10)$, the goal is to follow it with a speed of 1 m/sec. The corresponding output function can be constructed as

$$\overline{y} = \text{col}\left(\; x_2 - \sin x_1, x_3 - 10, x_1, x_{15} - \tfrac{\pi}{4} \; \right). \tag{23}$$

The initial position of the load in this scenario is considered as $x_\ell(0) = \text{col}(0, -10.1, 10)$, As shown in Figure 3, the load converges to the path. It can be seen in the figure that the quadrotor undergoes large rotations about the roll and pitch axis to force the load to approach the desired path γ and then maintains the load position on the desired path. Mathematically, the path following manifold $\Gamma^\star$ achieves stability, i.e., ξ- and ζ states converge[4]. The transformed states η and μ are shown in Figure 4, As seen in the figure, η_2 reaches the target value, while η_1 evolves in an unconstrained manner. The remaining states of the η-subsystem approach zero. It can be observed that η_6 exhibits sensitivity to additive sensor noise since it is computed by repeated differentiation of the load position. We underscore that irrespective of the noise in η_6, the load follows the path very precisely. Moreover, as seen in the second plot in Figure 4, the μ_1-state reaches the desired heading value, and μ_2 converges to zero. The simulation code is available online[5].

[4]These plots are not shown due to space limitations. For details, please refer to [24].

VI. EXPERIMENTAL RESULTS

In this section, we implement the proposed controller to assess its performance on a real cable-suspended aerial robotic platform, i.e., QDrone[6]. The experimental setup consists of a flying arena, a camera system, a UAV with a cable-suspended load, a ground station, and a WiFi router, as shown in Figure 5. The UAV used in this experimental work is a drone manufactured by Quanser, called QDrone. The physical dimensions of the Quanser QDrone UAV are 40 $\times$ 40 $\times$ 15 cm, and the cable length for this experiment is 40 cm. The rest of the parameters are shown in Table I.

In this experimental study, the goal is to follow the given path, a circle with a radius of 1m at 0.3m above ground level. When the experiment begins, the initial position of the UAV and the cable-suspended payload is on the ground with no tension in the cable. To ensure Assumption 1 is satisfied, the UAV ascends to a height such that the payload lifts off from the ground and the cable tension becomes non-zero. The load swing is considerably reduced before invoking our proposed path following controller. Figure 6 shows both the position of the UAV and the payload during the flight. Once the path following controller is enabled, first, the payload converges to the path and then traverses it. The controller gains are selected using classical control design methods and then carefully fine-tuned on the experimental hardware. For numerical values of the gains, please refer to [24]. At the termination of the mission, the autonomous landing mode of the quadrotor is activated.

A small error can be observed between the payload and the given path due to the presence of noise and state estimation error. The error in the x, y plane and z direction are shown separately in Figure 7. The error is initially large since the UAV and the payload is on the ground. After around 7 seconds, our proposed path following controller takes over, leading to a steady reduction in error. It can be seen from the figure that the controller performance is satisfactory in the presence of noise and delay inherent to the experimental setup.

Next, Figure 8 shows the control input generated by Quanser Qdrone. For the QDrone used in this experiment, the thrust and torque limits are 16 N and 0.8 N-m, respectively. It is clear from the figure that the actuation limits of the UAV system never exceed throughout the mission. We want to highlight that the proposed controller is enabled around 7 sec after the start of the mission. Hence, the results presented in this section are valid after that time.

[5]https://gitlab.com/a5akhtar/quadrotor-load-path-following.git
[6]https://www.quanser.com/products/qdrone/

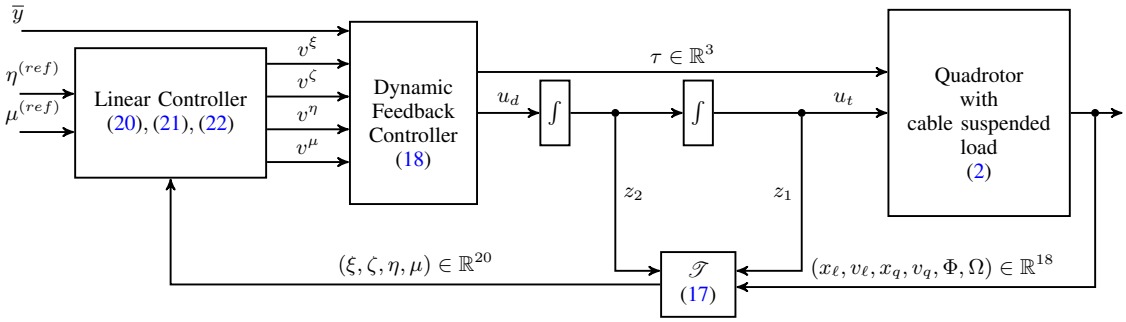

Fig. 2. The overall system architecture for the proposed controller design with the non-linear coordinate transformation.

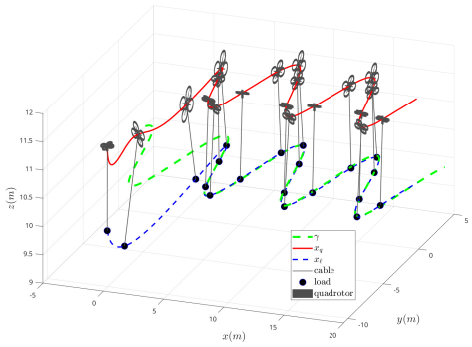

Fig. 3. The position of the UAV and the payload for a non-closed path.

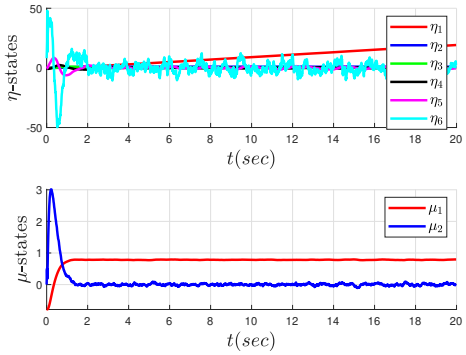

Fig. 4. Trajectories of η states and μ states in the presence of sensor noise and parametric uncertainties when following a non-closed curve.

VII. Conclusion

This paper considers the path following problem for a UAV quadrotor tethered to a load through an inelastic cable. A novel smooth dynamic feedback controller is proposed for a large class of embedded curves. The path following controller designed in this work has two distinguishing features: a) payload converges to the given path and attains path invariance; b) constraints on payload motion and orientation are satisfied while it follows the assigned path. The proposed path following control law is validated using both numerical simulations and real-world experiments.

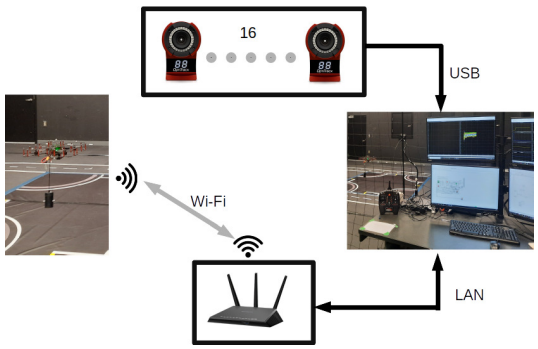

Fig. 5. An experimental setup based on the Quanser QDrone system.

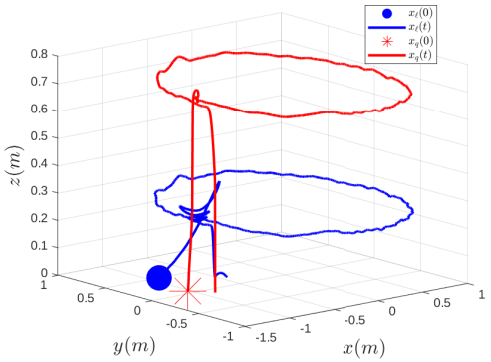

Fig. 6. Position of the payload and Quanser UAV in an indoor flight arena while following a circular path.

VIII. Appendix

A. Proof of Lemma IV.4

Proof. First, we prove that the vectors $d_\chi\alpha_1, d_\chi\alpha_2, \sigma'$ are not null vectors. Since, the curve is regular, $\sigma' \neq 0$. Moreover, Assumption 2 implies that for all $y \in \gamma$, ds_y is not rank deficient. As $dh_x = I$, chain rule can be used to show that for all $\chi^\star \in \Gamma$, $d_\chi\alpha$ is full rank. As $d_\chi\alpha_1, d_\chi\alpha_2$ are non-zero gradient vectors are gradient vectors and σ' is a tangent vector, this implies that $\text{span}\{d_\chi\alpha_1, d_\chi\alpha_2, \sigma'\} = \mathbb{R}^3$. This concludes the proof. □

B. Definition of Vector Relative Degree

Definition VIII.1. *Given a time-invariant, control-affine system with input vector* $u := [u_1, \ldots, u_m]^\top \in \mathbb{R}^m$ *and output*

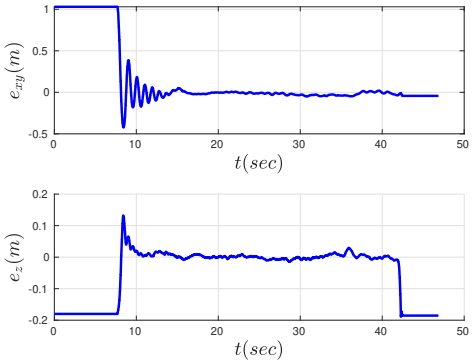

Fig. 7. Path following error in xy-plane and z-axis are shown in the figure.

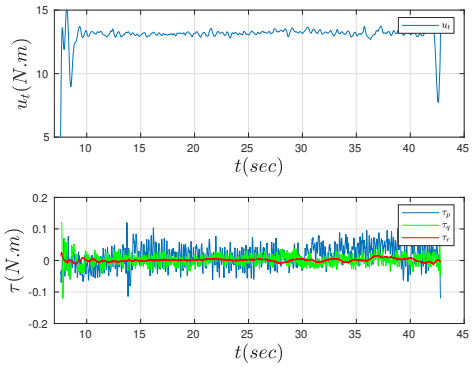

Fig. 8. Thrust control input u_t and control torques τ_p, τ_q, τ_r generated by the Quanser QDrone while following the assigned path.

vector $y := [y_1, \ldots, y_m]^\top \in \mathbb{R}^m$ *and consider smooth functions* $f : \mathbb{R}^n \to \mathbb{R}^n$, $g_i : \mathbb{R}^n \to \mathbb{R}^n$ *and* $h : \mathbb{R}^n \to \mathbb{R}^m$ *such that*

$$\dot{x} = f(x) + \sum_{i=1}^{m} g_i(x)u_i := f(x) + g(x)u, \tag{24}$$

and consider a smooth map,

$$y = h(x) = \begin{bmatrix} h_1(x) \\ \vdots \\ h_m(x) \end{bmatrix}, \text{ for all } y \in \mathbb{R}^m, \tag{25}$$

which is the output of the system. We can define an $m \times m$ *decoupling matrix,*

$$A(x) := \begin{bmatrix} L_{g_1}L_f^{r_1-1}h_1(x) & \cdots & L_{g_m}L_f^{r_1-1}h_1(x) \\ L_{g_1}L_f^{r_2-1}h_2(x) & \cdots & L_{g_m}L_f^{r_2-1}h_2(x) \\ \vdots & \ddots & \vdots \\ L_{g_1}L_f^{r_m-1}h_m(x) & \cdots & L_{g_m}L_f^{r_m-1}h_m(x) \end{bmatrix}. \tag{26}$$

The given system achieves a vector relative degree of $\{r_1, \ldots, r_m\}$ *at a point* x_0 *if*

1) $L_{g_j}L_f^k h_i(x) = 0$, *for all* $i \in \{1, 2, \ldots, m\}$, *for all* $j \in \{1, 2, \ldots, m\}$, *for all* $k < r_i - 1$, *and for all* x *in a neighborhood of* x_0.
2) *The decoupling matrix* $A(x)$ *is non-singular at* $x = x_0$.

REFERENCES

[1] S. Yang and B. Xian, "Exponential regulation control of a quadrotor unmanned aerial vehicle with a suspended payload," *IEEE Transactions on Control Systems Technology*, pp. 1–8, 2019. 1

[2] B. Xian, S. Wang, and S. Yang, "An online trajectory planning approach for a quadrotor uav with a slung payload," *IEEE Transactions on Industrial Electronics*, vol. 67, no. 8, pp. 6669–6678, 2020. 1

[3] K. Sreenath, N. Michael, and V. Kumar, "Trajectory generation and control of a quadrotor with a cable-suspended load - a differentially-flat hybrid system," in *2013 IEEE International Conference on Robotics and Automation*, pp. 4888–4895, May. 2013. 1, 2

[4] S. Yang and B. Xian, "Energy-based nonlinear adaptive control design for the quadrotor UAV system with a suspended payload," *IEEE Transactions on Industrial Electronics*, vol. 67, no. 3, pp. 2054–2064, 2020. 1, 2

[5] M. Guo, D. Gu, W. Zha, X. Zhu, and Y. Su, "Controlling a quadrotor carrying a cable-suspended load to pass through a window," *Journal of Intelligent & Robotic Systems*, 05 2019. 1, 2

[6] T. Chen and J. Shan, "Distributed tracking of a class of underactuated lagrangian systems with uncertain parameters and actuator faults," *IEEE Transactions on Industrial Electronics*, vol. 67, no. 5, pp. 4244–4253, 2020. 1

[7] A. Akhtar, C. Nielsen, and S. L. Waslander, "Path following using dynamic transverse feedback linearization for car-like robots," *IEEE Transactions on Robotics*, vol. 31, no. 2, pp. 269–279, Apr. 2015. 1, 3

[8] A. P. Aguiar, J. P. Hespanha, and P. V. Kokotović, "Performance limitations in reference tracking and path following for nonlinear systems," *Automatica*, vol. 44, no. 3, pp. 598–610, 2008. 1, 2

[9] C. Nielsen, C. Fulford, and M. Maggiore, "Brief paper: Path following using transverse feedback linearization: Application to a maglev positioning system," *Automatica*, vol. 46, no. 3, pp. 585–590, 2010. 1, 4

[10] A. Akhtar, S. Saleem, and S. L. Waslander, "Path following for a class of underactuated systems using global parameterization," *IEEE Access*, vol. 8, pp. 34 737–34 749, 2020. 1, 2, 3, 6

[11] D. C. Gandolfo, L. R. Salinas, A. Brandão, and J. M. Toibero, "Stable path-following control for a quadrotor helicopter considering energy consumption," *IEEE Transactions on Control Systems Technology*, vol. 25, no. 4, pp. 1423–1430, Jul. 2017. 1

[12] K. Sreenath, T. Lee, and V. Kumar, "Geometric control and differential flatness of a quadrotor uav with a cable-suspended load," in *52nd IEEE Conference on Decision and Control*, pp. 2269–2274, Dec. 2013. 1, 3

[13] A. Akhtar and S. L. Waslander, "Controller class for rigid body tracking on SO(3)," *IEEE Transactions on Automatic Control*, vol. 66, no. 5, pp. 2234–2241, 2021. 1

[14] T. Lee, "Geometric control of quadrotor uavs transporting a cable-suspended rigid body," *IEEE Transactions on Control Systems Technology*, vol. 26, no. 1, pp. 255–264, Jan. 2018. 1

[15] J. Zeng, P. Kotaru, and K. Sreenath, "Geometric control and differential flatness of a quadrotor uav with load suspended from a pulley," in *2019 American Control Conference (ACC)*, pp. 2420–2427, Jul. 2019. 1, 2

[16] P. Kotaru, G. Wu, and K. Sreenath, "Dynamics and control of a quadrotor with a payload suspended through an elastic cable," in *2017 American Control Conference (ACC)*, pp. 3906–3913, May. 2017. 1

[17] T. Lee, K. Sreenath, and V. Kumar, "Geometric control of cooperating multiple quadrotor uavs with a suspended payload," in *52nd IEEE Conference on Decision and Control*, pp. 5510–5515, Dec. 2013. 1, 2

[18] J. Zeng and K. Sreenath, "Geometric control of a quadrotor with a load suspended from an offset," in *2019 American Control Conference (ACC)*, pp. 3044–3050, Jul. 2019. 2

[19] S. Jia and J. Shan, "Finite-time trajectory tracking control of space manipulator under actuator saturation," *IEEE Transactions on Industrial Electronics*, vol. 67, no. 3, pp. 2086–2096, 2020. 2

[20] P. O. Pereira and D. V. Dimarogonas, "Pose and position trajectory tracking for aerial transportation of a rod-like object," *Automatica*, vol. 109, p. 108547, 2019. 2

[21] A. Akhtar, S. L. Waslander, and C. Nielsen, "Path following for a quadrotor using dynamic extension and transverse feedback linearization," in *51st IEEE Conference on Decision and Control (CDC)*, pp. 3551 –3556, Dec. 2012. 2, 3, 4, 5

[22] L. Qian and H. H. T. Liu, "Path-following control of a quadrotor uav with a cable-suspended payload under wind disturbances," *IEEE Transactions on Industrial Electronics*, vol. 67, no. 3, pp. 2021–2029, Mar. 2020. 2

[23] P. Cruz and R. Fierro, "Cable-suspended load lifting by a quadrotor uav: hybrid model, trajectory generation, and control," *Autonomous Robots*, vol. 41, pp. 1629 – 1643, 04 2017. 2, 3

[24] A. Akhtar, S. Saleem, and J. Shan, "Technical report: Path following of a quadrotor with a cable-suspended payload," York University, Toronto, Tech. Rep., 2021. [Online]. Available: http://adeelakhtar.com/assets/pdf/Technical_report_quadload_2021.pdf 3, 5, 6

[25] A. Akhtar, S. Waslander, and C. Nielsen, "Fault tolerant path following for a quadrotor," in *52nd IEEE Conference on Decision and Control (CDC)*, pp. 847–852, Dec. 2013. 4

[26] S. Sastry, *Nonlinear systems: analysis, stability, and control*. New York: Springer, 1999. 4

Adeel Akhtar (S'12 - M'18) his M.A.Sc. degree in ECE Department, from Univ. of Waterloo, Canada, in 2012. He received his Ph.D from Mechanical and Mechatronics Engineering Department, Univ. of Waterloo, Canada, in 2018.

Currently, he is a post-doctoral research scientist with ECE Department, at Univ. of California at Santa Cruz. Prior to that he held postdoctoral positions at the Univ. of Toronto, Canada, and York Univ., Canada.

Sajid Saleem (S'09 - M'14 - SM '20) received the M.S. degree in mathematics and the Ph.D. degree in ECE from the Georgia Institute of Technology, Atlanta, GA USA, in 2011 and 2013, respectively.

He is currently an Assistant Professor with the College of Computer Science and Engineering, University of Jeddah, Jeddah, Saudi Arabia.

His research interests include systems analysis, signal processing, and differential geometry.

Jinjun Shan (Senior Member, IEEE) received Ph.D. degree in spacecraft design from Harbin Institute of Technology, Harbin, China, in 2002.

He is currently a professor of Space Engineering and Chair of Dept. of Earth and Space Science and Engineering, York Univ., Toronto, Canada.

Dr. Shan was the recipient of Alexander von Humboldt Fellowship. and Japan Society for the Promotion of Science Fellowship in 2012.